



ELSEVIER

Available online at [www.sciencedirect.com](http://www.sciencedirect.com)

SCIENCE @ DIRECT®

Journal of Organometallic Chemistry 675 (2003) 21–34

Journal  
of Organometallic  
Chemistry[www.elsevier.com/locate/jorgchem](http://www.elsevier.com/locate/jorgchem)

# Reduction of the NO<sup>+</sup> ligand in ‘half-sandwich’ ruthenium derivatives

Pietro Diversi<sup>a,\*</sup>, Marco Fontani<sup>b</sup>, Melania Fuligni<sup>a</sup>, Franco Laschi<sup>b</sup>,  
Fabio Marchetti<sup>a</sup>, Simona Matteoni<sup>a</sup>, Calogero Pinzino<sup>c</sup>, Piero Zanello<sup>b</sup>

<sup>a</sup> Dipartimento di Chimica e Chimica Industriale dell'Università di Pisa, Via Risorgimento 35, 56126 Pisa, Italy

<sup>b</sup> Dipartimento di Chimica, Università di Siena, Via Aldo Moro, 53100 Siena, Italy

<sup>c</sup> Istituto per i Processi Chimico-Fisici del C.N.R., Area della Ricerca di Pisa, Via G. Moruzzi 1, 56124 Pisa, Italy

Received 8 January 2003; received in revised form 17 March 2003; accepted 17 March 2003

## Abstract

The reduction of the tetrafluoroborate salts of the ruthenium nitrosyl dicationic  $[\text{Ru}(\eta^5\text{-C}_5\text{R}_5)(\text{NO})(\text{L})_2]^{2+}$  ( $\text{R} = \text{Me}$ ,  $\text{L} = \text{PMe}_3$ , **1a**;  $\text{PMe}_2\text{Ph}$ , **1b**;  $\text{R} = \text{H}$ ,  $\text{L} = \text{PPh}_3$ , **2d**) and monocationic complexes  $[\text{Ru}(\text{Me})\text{Cp}^*(\text{NO})\text{L}]^+$  ( $\text{L} = \text{PMe}_3$ , **3a**;  $\text{PMe}_2\text{Ph}$ , **3b**) ( $\text{Cp}^* = \eta^5\text{-C}_5\text{Me}_5$ ) has been studied by electrochemical and spectroscopic (IR, NMR, EPR) techniques. The nitrosyl complexes **1a**, **1b** and **2d** exhibit two successive one-electron cathodic processes due to the sequential reduction of coordinated NO<sup>+</sup> to NO• and NO<sup>-</sup>, respectively. Chemical reduction yields products of rearrangement of the intermediates which have been spectroscopically characterized. EPR studies and theoretical calculations show that in the first one-electron reduction product the electron interacts with the NO nitrogen atom and that the RuNO moiety presents significant distortion from linearity. The X-ray structure of the related  $[\text{Ir}(\text{Me})_2\text{Cp}^*(\text{NO})]\text{BF}_4$  has been determined.

© 2003 Elsevier Science B.V. All rights reserved.

**Keywords:** Nitrosyls; Ruthenium complexes; Electrochemistry; EPR spectroscopy

## 1. Introduction

Metal nitrosyl complexes have recently attracted renewed attention because of the important role that NO plays in air pollution [1], as models for metal enzymes [2] and in a number of physiological processes [3]. Such an interest is testified by the recent publication of a thematic issue dedicated to the nitric oxide chemistry [4].

An important area of research for nitrosyl complexes is concerned with the geometric and electronic features of the NO ligand: in this context, reduction of 18e metal nitrosyl complexes allows the study of the structural modification of the NO ligand and the character of the orbital populated by the extra electron(s).

A survey of the literature indicates that most often, as a result of one-electron reduction, a substantial localisa-

tion of the unpaired electron on the NO occurs, as it results mainly from EPR and IR spectroscopy: indeed few examples of structurally characterised 19e complexes have been reported, and only in one case the corresponding 18 and 19e systems have been isolated and fully characterised [5e]. Apparently the iridium {MNO}<sup>7-</sup>-type [6] nitrosyl derivatives  $[\text{Ir}(\text{Me})\text{Cp}^*(\text{NO})(\text{L})]\text{BF}_4$  ( $\text{L} = \text{PMePh}_2$ ,  $\text{PMe}_2\text{Ph}$ ,  $\text{PMe}_3$ ), prepared by one-electron reduction of the corresponding  $[\text{Ir}(\text{Me})\text{Cp}^*(\text{NO})(\text{L})](\text{BF}_4)_2$  complexes, seem to belong to this class of complexes [7]. Indeed, although these compounds have not been structurally characterised, the hyperfine structure in the EPR spectra shows that the unpaired electron interacts with the iridium nucleus (no hyperfine coupling to <sup>14</sup>N was observed).

In this context the recent availability of the new {MNO}<sup>6-</sup>-type nitrosyl complexes  $[\text{Ru}(\eta^5\text{-C}_5\text{R}_5)(\text{NO})(\text{L})_2](\text{BF}_4)_2$  ( $\text{R} = \text{Me}$ ,  $\text{H}$ ;  $\text{L} = \text{PMe}_3$ ,  $\text{PMe}_2\text{Ph}$ ;  $\text{PPh}_3$ ) and  $[\text{Ru}(\text{Me})\text{Cp}^*(\text{NO})(\text{L})]\text{BF}_4$  ( $\text{L} = \text{PMe}_3$ ,  $\text{PMe}_2\text{Ph}$ ;  $\text{Cp}^* = \eta^5\text{-C}_5\text{Me}_5$ ), which have been prepared by reaction of the corresponding  $[\text{Ru}(\text{Me})\text{Cp}^*(\text{L})_2]$  derivatives [8] with

\* Corresponding author. Tel.: +39-50-918-225; fax: +39-50-918-410.

E-mail address: [div@deci.unipi.it](mailto:div@deci.unipi.it) (P. Diversi).

NOBF<sub>4</sub>, gives the opportunity to compare the behaviour of the iridium and ruthenium M–N–O systems towards reduction.

A number of previous studies exist on the electrochemical and chemical reduction of ruthenium(II) nitrosyl complexes [9], mainly coordination derivatives like [Ru(Cl)(NO)(bpy)<sub>2</sub>]<sup>2+</sup> (bpy = 2,2'-bipyridine) [9a], [Ru(hedta)(NO)] (hedta<sup>3-</sup> = N-(hydroxyethyl)ethylenediaminetriacetate) [9c], [Ru(NO)(H<sub>2</sub>O)(bpy)<sub>2</sub>]<sup>3+</sup> [9d], and [Ru(L)(NO)(trpy)]<sup>3+</sup> (trpy = 2,2':6',2''-terpyridyl) [9e]. However since ruthenium complexes of the {MNO}<sup>6</sup>-type strongly coordinate NO but readily release NO• after one-electron reduction, there is a paucity of EPR reports of nitrosyls with the unpaired electron located mainly on the nitrogen atom [9]. For the few {RuNO}<sup>7</sup>-type complexes, which have been isolated, although not structurally characterised, like [Ru(py)<sub>2</sub>(NO)Cl]I [10] and [Ru(py)<sub>4</sub>(NO)Cl]PF<sub>6</sub> [11], the experimental data are consistent with a bent nitrosyl ligand and the unpaired electron is best considered as occupying an antibonding π\*(NO) orbital. However, as far as we know, no organometallic nitrosyl compound of ruthenium was studied in this perspective. In this paper we report the results obtained in the study of electrochemical and chemical reduction of the above cited ruthenium dicationic and monocationic complexes [8].

## 2. Results and discussion

### 2.1. Electrochemical studies

The electrochemical behaviour of the nitrosyl complexes [Ru(η<sup>5</sup>-C<sub>5</sub>R<sub>5</sub>)(NO)(L)<sub>2</sub>](BF<sub>4</sub>)<sub>2</sub> (R = Me, L = PMe<sub>3</sub>, **1a**; PMe<sub>2</sub>Ph, **1b**; R = H, L = PPh<sub>3</sub>, **2d**) and [Ru(Me)Cp\*(NO)L]BF<sub>4</sub> (L = PMe<sub>3</sub>, **3a**; PMe<sub>2</sub>Ph, **3b**) has been studied by cyclic voltammetry and controlled potential coulometry [12].

As illustrated in Fig. 1, [RuCp\*(NO)(PMe<sub>3</sub>)<sub>2</sub>](BF<sub>4</sub>)<sub>2</sub> (**1a**) exhibits in acetone solution two reduction processes ( $E_{1'}^{\circ} = -0.08$  V;  $E_{2'}^{\circ} = -0.77$  V) with features of chemical reversibility in the cyclic voltammetric time scale ( $i_{pa}/i_{pc}$  constantly equal to 1).

Controlled potential coulometry for the first reduction step ( $E_w = -0.3$  V) consumes one electron per molecule. As a consequence of exhaustive reduction the original yellow-ocre colour turns red–brown, and the resulting solution displays in cyclic voltammetry a voltammetric profile quite complementary to that illustrated in Fig. 1, thus confirming the chemical reversibility of the [RuCp\*(NO)(PMe<sub>3</sub>)<sub>2</sub>]<sup>2+</sup>/[RuCp\*(NO)(PMe<sub>3</sub>)<sub>2</sub>]<sup>•+</sup> reduction also in the long times of macroelectrolysis.

The assignment of the nature of the two reduction processes is not straightforward because of the con-

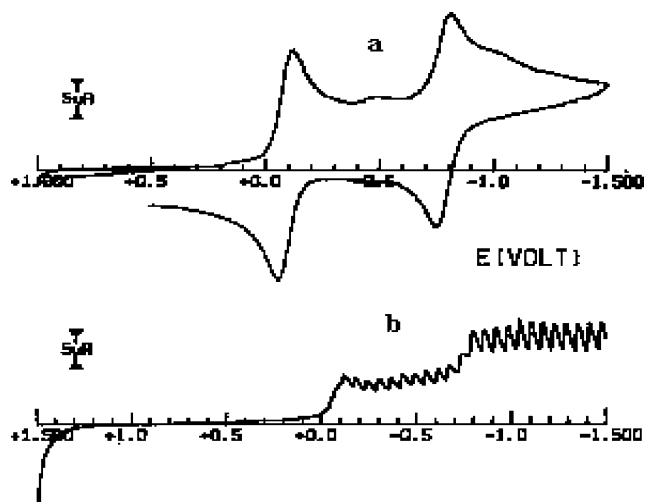


Fig. 1. Cyclic (a) and hydrodynamic (b) voltammetric responses recorded at a platinum electrode on an acetone solution of **1a** ( $1.0 \times 10^{-3}$  mol dm<sup>-3</sup>) containing [NBu<sub>4</sub>]PF<sub>6</sub> (0.2 mol dm<sup>-3</sup>) as supporting electrolyte. Scan rates: (a) 0.2 V s<sup>-1</sup>; (b) 0.01 V s<sup>-1</sup>.  $T = 20$  °C.

comitant presence of the two redox-active moieties Ru(II) and NO<sup>+</sup>.

In this connection Fig. 2 shows the X-band EPR spectra recorded on an acetone solution of [RuCp\*(NO)(PMe<sub>3</sub>)<sub>2</sub>]<sup>•+</sup> electrogenerated at  $-20$  °C ( $E_w = -0.3$  V). At low temperature (Fig. 2a), the first derivative spectrum exhibits a resolved anisotropic line-shape typical of  $S = 1/2$  paramagnetic species [8,13]. A main broad 1:1:1 hyperfine three-signal system appears in the low-field region, the second derivative revealing the presence of two overlapped 1:1:1 triplets. It is noted that all the  $g_i$  values significantly differ from the  $g$  value of free electron (Table 1).

In turn, the second derivative low-field spectral region puts in evidence that each triplet is further splitted in a poorly resolved 1:2:1 superhyperfine triplet, whereas in the high field region ( $g_3$ ) the two (1:1:1 + 1:2:1) triplets display larger hpf resolution.

Computer simulation [14] allows the X-band parameters to be defined in terms of a poorly resolved rhombic structure ( $g_1 \cong g_2 > g_3 \neq g_{\text{electron}} = 2.0023$ ),

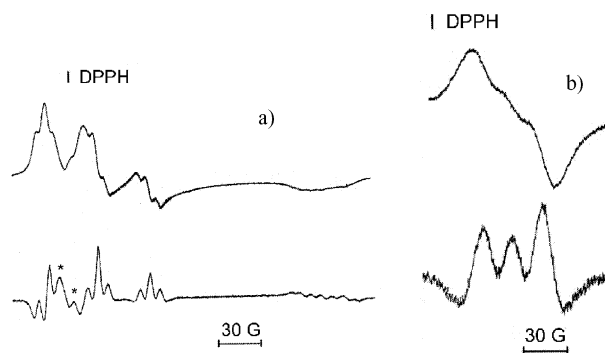


Fig. 2. X-band EPR spectra of [RuCp\*(NO)(PMe<sub>3</sub>)<sub>2</sub>]<sup>•+</sup>. (a) At 100 K; (b) at 210 K. First (upper) and second (lower) derivative modes.

Table 1

Temperature dependent X-band EPR parameters of the paramagnetic Ru(II) species derived by the one-electron electrochemical reduction of **1a**, **1b**, **2d**<sup>a</sup>

Complex	$g_1$	$g_2$	$g_3$	$\langle g \rangle$	$a_1^b$	$a_2^b$	$a_3^b$	$\langle a \rangle^b$	$g_{\text{iso}}$	$a_{\text{iso}}$
[RuCp*(NO)(PMe <sub>3</sub> ) <sub>2</sub> ] <sup>•+</sup>	2.001(4)	1.994(4)	1.912(4)	1.969(5)	6(3)	33(3)	13(3)	17(3)	1.972(5) <sup>c</sup>	20(3)
[RuCp*(NO)(PMe <sub>2</sub> Ph) <sub>2</sub> ] <sup>•+</sup>	1.996(5)	1.996(5)	1.964(5)	1.985(5)	$\leq \Delta H_1$	6(3)	7(3)	$\leq \Delta H_{\text{h}}$	2.020(5) <sup>d</sup>	$\leq \Delta H_{\text{iso}}$
[RuCp(NO)(PPh <sub>3</sub> ) <sub>2</sub> ] <sup>•+</sup>	1.995(6)	1.995(6)	1.896(6)	1.962(6)	$\leq \Delta H_1$	28.5	$\leq \Delta H_{\text{h}}$	$\leq \Delta H_{\text{aniso}}$	–	$\leq \Delta H_{\text{iso}}$
					$\leq \Delta H_1$		$\leq \Delta H_{\text{h}}$	$\leq \Delta H_{\text{aniso}}$		$\leq \Delta H_{\text{iso}}$

<sup>a</sup>  $\langle g \rangle = (g_1 + g_2 + g_3)/3$ ,  $(g_{\parallel} + 2g_{\perp})/3$ ;  $\langle a \rangle = (a_1 + a_2 + a_3)/3$ ,  $(a_{\parallel} + 2a_{\perp})/3$ ;  $(a, g)_{\parallel}$  values refer to the high field spectral region;  $(a, g)_{\perp}$  values refer to the low field spectral regions.

<sup>b</sup> Upper values relevant to <sup>14</sup>N hpf couplings, lower values relevant to <sup>31</sup>P shpf couplings;  $a_i$  in Gauss.

<sup>c</sup>  $T = 210$  K.

<sup>d</sup>  $T = 200$  K.

with the unpaired electron mainly located on the NO ligand. In fact, the narrower 1:2:1 triplets arise from the minor interaction of the unpaired electron with two nearly magnetically equivalent P nuclei. Accordingly no ruthenium satellite peaks could be detected (<sup>101</sup>Ru: I = 3/2, 12.7%; <sup>103</sup>Ru: I = 5/2, 17.1%) as a consequence of noticeable anisotropic line broadening. The EPR lineshape analysis indicates that the actual SOMO is basically constituted by the nitrogen and phosphorus np orbitals with a very minor contribution of the ruthenium 4d orbitals [9f].

It is noted that, even if the paramagnetic parameters are substantially similar the actual frozen lineshape obtained on Me<sub>2</sub>CO solution, the spectrum somewhat differs from that recorded on the monocation [RuCp\*(NO)(PMe<sub>3</sub>)<sub>2</sub>]<sup>•+</sup> obtained by chemical reduction in CH<sub>2</sub>Cl<sub>2</sub> solution (see infra), likely because of the different solute–solvent interaction. Moreover, close inspection of the low temperature second derivative lineshape evidences additional EPR features of minor spectral intensity, namely two distinct peaks (see starred peaks in Fig. 2) positioned in the low-field region and overlapped onto the main  $m_1 = -1$  N signal. As the Scheme 3 suggests, such spectral pattern could testify for the presence of a second minor ruthenium paramagnetic species.

On rising the temperature at the glassy-fluid transition, the anisotropic spectrum collapses in a broad isotropic signal ( $T = 210$  K,  $\Delta H_{\text{iso}} = 57(5)$  G), which displays poor nitrogen resolution and no <sup>31</sup>P shpf resolution ( $\Delta H_{\text{iso}} > a_{\text{iso}}$ ) (Fig. 1b). The EPR parameters of the isotropic NO hpf resolution are consistent with those of the corresponding glassy state, but with some temperature dependent line broadening due to the effective fastening of the molecular dynamics. At  $T = 285$  the isotropic spectrum becomes very poorly resolved ( $g_{\text{iso}}(285 \text{ K}) = 1.965(4)$ ;  $\Delta H_{\text{iso}}(285 \text{ K}) = 68(5)$  G;  $a_{\text{iso}} = 20(5)$  G from second derivative analysis). Quick re-freezing of the fluid solution quantitatively restores the previous glassy spectrum, thus indicating the high

stability of the electrogenerated monocation [RuCp\*(NO)(PMe<sub>3</sub>)<sub>2</sub>]<sup>•+</sup>.

In conclusion, the spectroscopic data indicate that the first reduction process illustrated in Fig. 1 is substantially centred on the nitrosyl ligand. No further experimental support on the nature of the second reduction could be gained because of the fast re-oxidation of the electrogenerated neutral product likely triggered by traces of dioxygen.

The redox propensity of [RuCp\*(NO)(PMe<sub>2</sub>Ph)<sub>2</sub>](BF<sub>4</sub>)<sub>2</sub> (**1b**) looks like slightly more complicated than that of **1a**; in fact, as shown in Fig. 3, it apparently displays three reduction processes.

Controlled potential coulometry ( $E_w = -0.2$  V) proved that the first reduction ( $E^{\circ'} = 0.00$  V), which at room temperature exhibits a good extent of chemical reversibility, involves a one-electron process. In contrast, the subsequent cathodic process ( $E_p = -0.61$  V), which conceivably parallels the second reduction of **1a**, is complicated by chemical reactions that generate a further reducible byproduct ( $E_p = -0.93$  V).

Low temperature ( $-20$  °C) exhaustive electrolysis for the first reduction process causes a colour change from yellow-ocre to green. The resulting monocation [RuCp\*(NO)(PMe<sub>2</sub>Ph)<sub>2</sub>]<sup>•+</sup> is sufficiently stable to be studied by X-band EPR spectroscopy (Fig. 4). The broad glassy spectrum can be explained in terms of partially resolved axial line shape ( $g_{\perp} > g_{\parallel} \neq g_{\text{electron}}$ ) in that it exhibits the well separated nitrogen hpf triplet only in the perpendicular region. The low-field spectral region could likely mask two  $g_2$  and  $g_3$  closely overlapped absorptions (here  $g_2 \cong g_3$  as  $g_{\parallel}$ ) due to significant anisotropic line-broadening. Accordingly, no shpf resolution of the two <sup>31</sup>P phosphine nuclei is detected ( $\Delta H_{\perp} > a_{\perp}(\text{<sup>31</sup>P})$ ). On the other hand, the parallel signal is very poorly resolved. Also in this case the EPR parameters suggest that the unpaired electron mainly interacts with the NO ligand, with a minor coupling with the phosphine moiety.

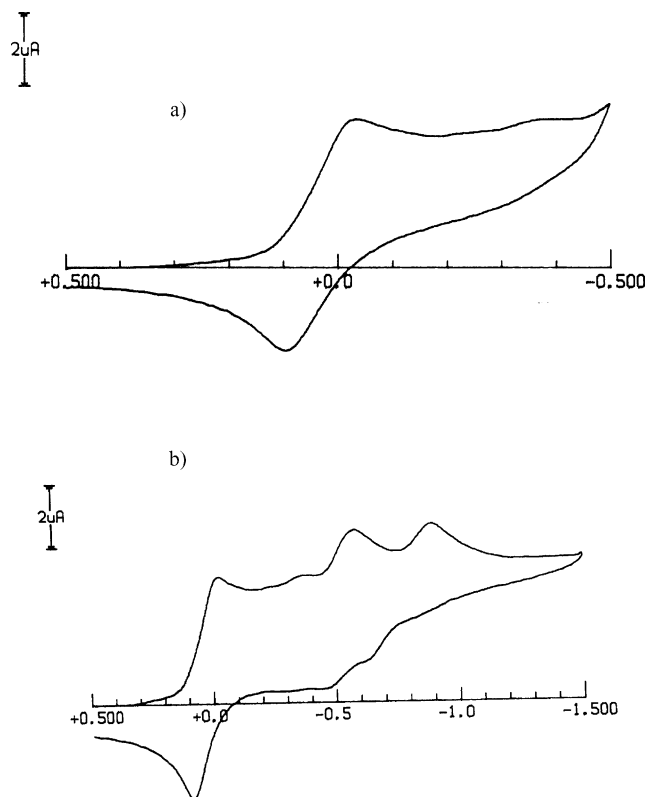


Fig. 3. Cyclic voltammograms recorded at a platinum electrode on an acetone solution of **1b** ( $1.1 \times 10^{-3} \text{ mol dm}^{-3}$ ).  $[\text{NBu}_4]\text{PF}_6$  ( $0.2 \text{ mol dm}^{-3}$ ) supporting electrolyte. Scan rates: (a)  $0.2 \text{ V s}^{-1}$ ; (b)  $0.02 \text{ V s}^{-1}$ .  $T = 20^\circ\text{C}$ .

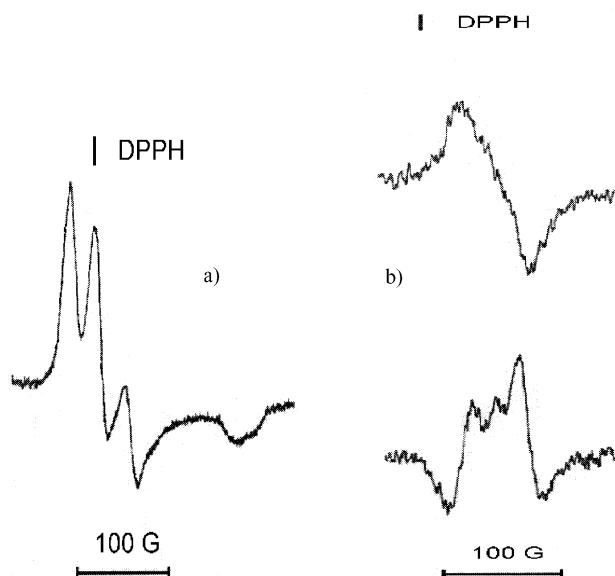


Fig. 4. X-band EPR spectra of an acetone solution of  $[\text{RuCp}^*(\text{NO})(\text{PMe}_2\text{Ph})_2]^{\bullet+}$ . (a) 100 K, first derivative; (b) 200 K. First (upper) and second (lower) derivative modes.

At the glassy-fluid transition the anisotropic spectrum evolves in a broad and poorly resolved signal. No well separated nitrogen hpf couplings are evident from the

better resolved second derivative mode, while the phosphine moieties coupling is not detected. Also in this case re-freezing the fluid solution restores the original frozen spectrum, indicating significant stability of the monocation.

Finally, in spite of the apparent complex cyclic voltammetric profile exhibited by  $[\text{RuCp}(\text{NO})(\text{PPh}_3)_2](\text{BF}_4)_2$  (**2d**) (Fig. 5), the cathodic path can be again viewed as two separated one-electron reductions as already described for **1a** (two reversible reductions) and **1b** (two reductions, the second of which is accompanied by chemical complication), but in this case the chemical complication is coupled to the first reduction. As a matter of fact, the first reduction ( $E^{\circ'} = -0.17 \text{ V}$ ) is partially chemically reversible (for example,  $i_{\text{pa}}/i_{\text{pc}} = 0.5$  at  $0.02 \text{ V s}^{-1}$ ). Based on the relative peak heights, we tentatively assign the second cathodic process ( $E_p = -0.44 \text{ V}$ ) to the generated byproduct, whereas the third cathodic step ( $E_p = -0.88 \text{ V}$ ) would correspond to the second main reduction.

Controlled potential coulometry in correspondence with the first reduction ( $E_w = -0.7 \text{ V}$ ) consumes  $1.2 \div 1.3$  electrons/molecule, confirming the formation of reducible byproducts.

Also in this case, low temperature electrogeneration ( $-20^\circ\text{C}$ ) of the corresponding monocation  $[\text{RuCp}(\text{NO})(\text{PPh}_3)_2]^{\bullet+}$  permits its relative characterisation by EPR spectroscopy (Fig. 6). The glassy spectrum exhibits pseudo-axial resolution ( $g_{\perp} > g_{\parallel}$ ), with the two  $g_1$  and  $g_2$  low field spectral regions being quite overlapped ( $g_1 \cong g_2$  as  $g_{\parallel}$ ). In this case, only the main anisotropic NO features are detectable as five partially overlapped nitrogen hpf peaks in the second derivative mode. In fact, the high field region exhibits a broad and unresolved signal both in the first and second derivative modes. At the glassy-fluid transition the anisotropic signal disappears and the fluid solution becomes EPR mute. Such a behaviour has to be attributed to important geometrical distortions of the monocation largely affecting the overall temperature dependent lineshape, rather than to its chemical instability, in that the quick re-freezing of the solution restores the original glassy lineshape [15].

Finally, we have studied the redox behaviour of the monocation derivatives  $[\text{Ru}(\text{Me})\text{Cp}^*(\text{NO})\text{L}]\text{BF}_4$  ( $\text{L} = \text{PMe}_3$ , **3a**;  $\text{PMe}_2\text{Ph}$ , **3b**). The cyclic voltammetric profile of  $[\text{Ru}(\text{Me})\text{Cp}^*(\text{NO})(\text{PMe}_3)]\text{BF}_4$  (**3a**) (Fig. 7) put in evidence a main reduction process with features of chemical reversibility ( $E^{\circ'}_1 = -0.80 \text{ V}$ ). The minor peak-systems at less negative potential values ( $E^{\circ'} = -0.08 \text{ V}$  and a shoulder at  $-0.7 \text{ V}$ ) are likely to be attributed to impurities of  $[\text{RuCp}^*(\text{NO})(\text{PMe}_3)_2](\text{BF}_4)_2$  (**1a**). In fact, controlled potential exhaustive electrolysis at potentials corresponding to the first minor reduction process ( $E_w = -0.40 \text{ V}$ ) consumes  $0.2\text{--}0.3$  electrons/molecule of **3a**, and the resulting solution affords an X-

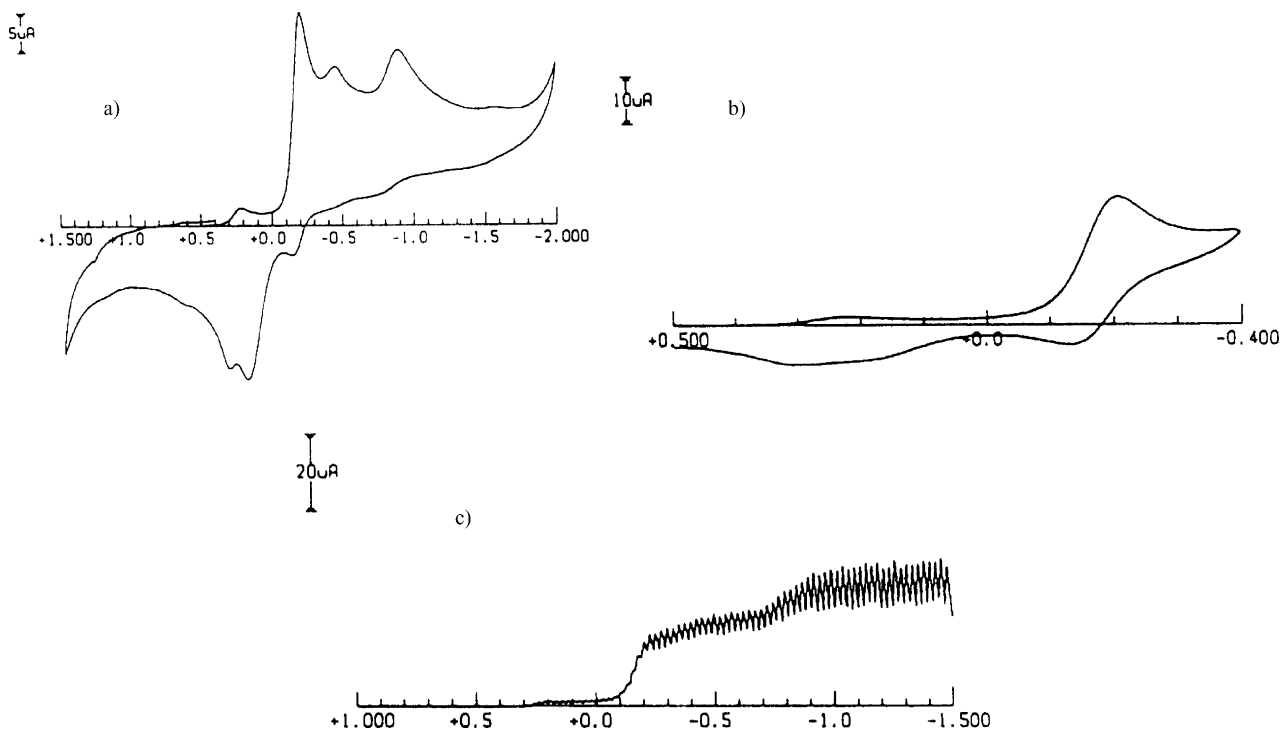


Fig. 5. Cyclic (a, b) and hydrodynamic (c) voltammograms recorded at a platinum electrode on a acetone solution of **2d** ( $1.1 \times 10^{-3}$  mol dm $^{-3}$ ). [NBu $_4$ ]PF $_6$  (0.2 mol dm $^{-3}$ ) supporting electrolyte. Scan rates: (a) 0.2 V s $^{-1}$ ; (b, c) 0.02 V s $^{-1}$ .  $T = 20$  °C.

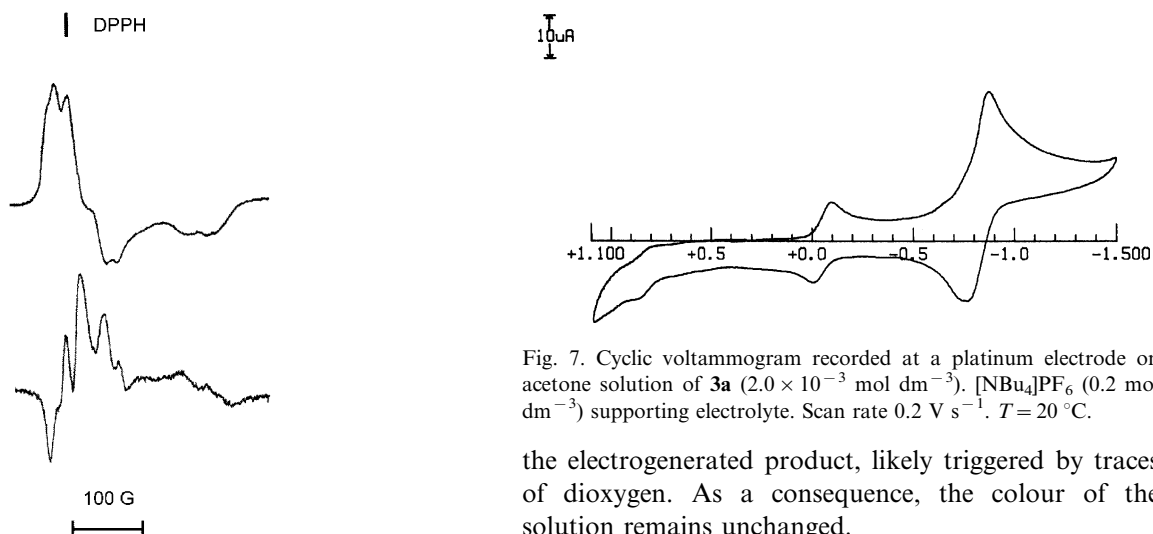


Fig. 6. X-band EPR spectra of the one-electron reduction product of **2d** in acetone at 104 K. First (upper) and second (lower) derivative modes.

band EPR spectrum which is basically consistent with the spectra found for the above discussed ruthenium paramagnetic systems, although is bad resolved and difficult to understand because of the extreme lability of the product.

Unfortunately, the subsequent exhaustive electrolysis in correspondence of the main cathodic process ( $E_w = -1.1$  V) did not allow the determination of the relative number of electrons because of the easy re-oxidation of

Fig. 7. Cyclic voltammogram recorded at a platinum electrode on acetone solution of **3a** ( $2.0 \times 10^{-3}$  mol dm $^{-3}$ ). [NBu $_4$ ]PF $_6$  (0.2 mol dm $^{-3}$ ) supporting electrolyte. Scan rate 0.2 V s $^{-1}$ .  $T = 20$  °C.

the electrogenerated product, likely triggered by traces of dioxygen. As a consequence, the colour of the solution remains unchanged.

[Ru(Me)Cp\*(NO)(PMe $_2$ Ph)]BF $_4$  (**3b**) also presents a cathodic process ( $E^{\circ'} = -0.97$  V) possessing features of partial chemical reversibility. Controlled potential electrolysis indicates that such a process involves a two-electron step in that it consumes  $1.8 \div 2.0$  electrons per ion. In confirmation, the monoanion electrogenerated at low temperature ( $-20$  °C) results EPR mute.

The different behaviour exhibited by the monocations with respect to the dications substantially reflects the different charge carried by the ions rather than the inductive effects of the ligands, as shown also by the similarity of the reduction potentials of [RuCp\*(NO)-(PMe $_3$ ) $_2$ ] $^{*+}$  and [Ru(Me)Cp\*(NO)(PMe $_3$ )] $^+$ .

## 2.2. Chemical reduction

The chemical reduction of  $[\text{RuCp}^*(\text{NO})(\text{L})_2](\text{BF}_4)_2$  ( $\text{L} = \text{PMe}_3$ , **1a**;  $\text{PMe}_2\text{Ph}$ , **1b**) and  $[\text{RuCp}(\text{NO})(\text{PPh}_3)_2](\text{BF}_4)_2$  (**2d**) with  $\text{CoCp}_2$  in  $\text{CH}_2\text{Cl}_2$  has been monitored in the cavity of a EPR spectrometer at different temperatures. Cobaltocene was used in less than the equimolar amounts in order to minimize any interference problem which could result by the presence of this paramagnetic species remaining after the one-electron reduction. Soon after the mixing of the reagents at low temperature (173 K) a signal was observed, which became more and more intense in the course of few hours, then it began to decrease. The signal disappeared only after some hours at room temperature. This may be due to the instability of the one-electron reduction product, but also further reduction to a diamagnetic species cannot be ruled out since cobaltocene, being far more soluble than the dications in  $\text{CH}_2\text{Cl}_2$ , was largely in excess in solution during the reaction.

In the case of **1a** and **1b** the EPR spectrum of the reduction products in solution (223 K) consists of a triplet showing a significant interaction of the unpaired electron with the  $^{14}\text{N}$  nucleus of the nitrosyl ligand. The spectrum of the frozen solution recorded at 113 K presents a well resolved structured signal of rhombic symmetry, which can be simulated by taking in account the hyperfine coupling to the nitrogen nucleus. The solution and the frozen spectra are reported in Fig. 8 in the case of **1a** as an example. The parameters obtained by simulation [16] are:  $g_{\text{iso}} = 1.975$ ,  $a_{\text{iso}} = 18.44$  G,  $g_1 = 2.0070$ ,  $g_2 = 2.0020$ ,  $g_3 = 1.9184$ ;  $a_1 = 11.53$  G,  $a_2 = 33.73$  G,  $a_3 = 12.01$  G. Since these parameters are almost the same as those of the electrochemically generated one-electron reduction product (Table 1), taking also in account the different solvent and resolution, the paramagnetic species was identified as  $[\text{RuCp}^*(\text{NO})(\text{PMe}_3)_2]^{\bullet+}$ , which should be better con-

sidered as a 18e ion complex since the unpaired electron interacts essentially with the nitrogen atom. The EPR spectra of the reduction product of **1b** are quite similar and the pertinent parameters are reported in Table 2.

Reduction of  $[\text{RuCp}(\text{NO})(\text{PPh}_3)_2](\text{BF}_4)_2$  (**2d**) shows some differences with respect to the previous cases. The EPR spectrum in solution (223 K) of the reduction mixture shows a single line, where no interaction with nitrogen is visible because of the width of the signal (it is to be remembered that in solution the electrochemically generated reduction product does not show any signal at all). Finally as shown in Fig. 9, the spectrum of the frozen solution at 113 K presents a structured signal, which may be interpreted in terms of rhombic symmetry as in the above cases. The parameters are the following:  $g_{\text{iso}} = 1.959$ ,  $g_1 = 2.0115$ ,  $g_2 = 1.9832$ ,  $g_3 = 1.9001$ ,  $a_1 = 16.30$  G,  $a_2 = 20.96$  G,  $a_3 = 22.88$  G,  $\langle g \rangle = 1.9649$ , where the hyperfine interaction has been assigned to the nitrogen atom of the nitrosyl ligand. After one day at room temperature no signal is present anymore. The active species has been identified as the one-electron reduction product  $[\text{RuCp}^*(\text{NO})(\text{PPh}_3)_2]^{\bullet+}$ .

In conclusion the compounds  $[\text{RuCp}^*(\text{NO})(\text{L})_2]^{\bullet+}$  ( $\text{L} = \text{PMe}_3$ ,  $\text{PMe}_2\text{Ph}$ ) and  $[\text{RuCp}(\text{NO})(\text{PPh}_3)_2]^{\bullet+}$  can be described as 18e complexes in which the nitrosyl ligand appears to be reduced. Since the ruthenium nitrosyl moiety is presumably linear in the dications **1a**, **1b** and **2d** (see Section 2.3) the one-electron reduction and subsequent re-oxidation may be viewed as proceeding with flipping of the nitrosyl system back and forth between the linear and bent structures. It is may be useful to compare the spectroscopic behaviour of these ruthenium complexes (see Table 2) and of the 19e iridium analogs,  $[\text{Ir}(\text{Me})\text{Cp}^*(\text{NO})(\text{L})]\text{BF}_4$ , cited above [7], which to the contrary may be interpreted in terms of the unpaired electron interacting significantly with the metal centre and poorly with the nitrosyl ligand.

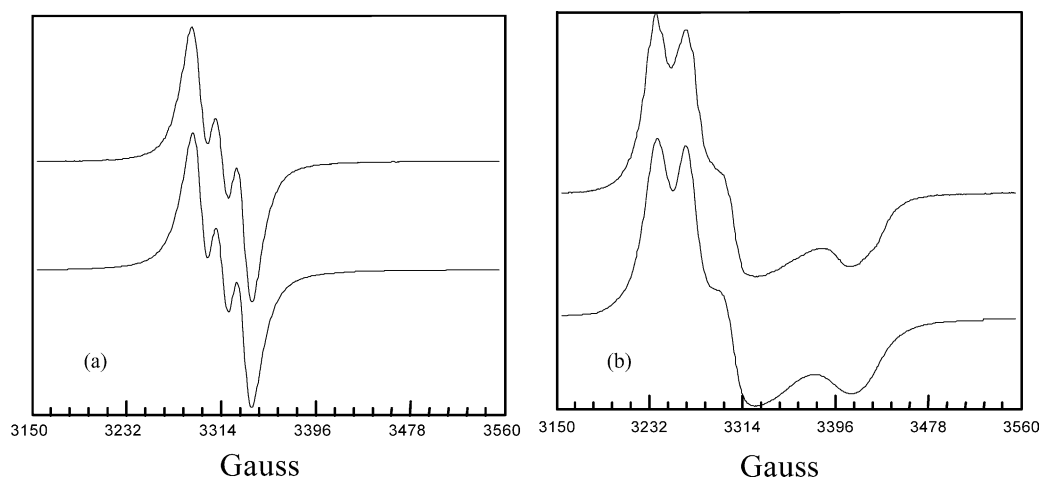


Fig. 8. X-band EPR observed (upper) and simulated (lower) spectra obtained by reduction of **1a** with  $\text{CoCp}_2$  in  $\text{CH}_2\text{Cl}_2$ : (a) at 223 K; (b) at 113 K.

Table 2  
X-band EPR parameters of the reduction products of **1a**, **1b**, **2d** with CoCp<sub>2</sub>

Species	$g_1^a$	$g_2^a$	$g_3^a$	$\langle g \rangle^a$	$a_1$ (G) <sup>a</sup>	$a_2$ (G) <sup>a</sup>	$A_3$ (G) <sup>a</sup>	$a_{iso}$ (G) <sup>b</sup>	$g_{iso}^b$
[RuCp*(NO)(PMe <sub>3</sub> ) <sub>2</sub> ] <sup>•+</sup>	2.0070	2.0020	1.9184	1.976	11.53	33.73	12.01	18.44	1.975
[RuCp*(NO)(PMe <sub>2</sub> Ph) <sub>2</sub> ] <sup>•+</sup>	2.0004	1.9983	1.9152	1.970	10.63	33.78	10.69	18.20	1.9712
[RuCp(NO)(PPh <sub>3</sub> ) <sub>2</sub> ] <sup>•+</sup>	2.0115	1.9832	1.9001	1.965	16.30	20.96	22.88	–	1.959

<sup>a</sup>  $T = 223$  K.

<sup>b</sup>  $T = 113$  K.

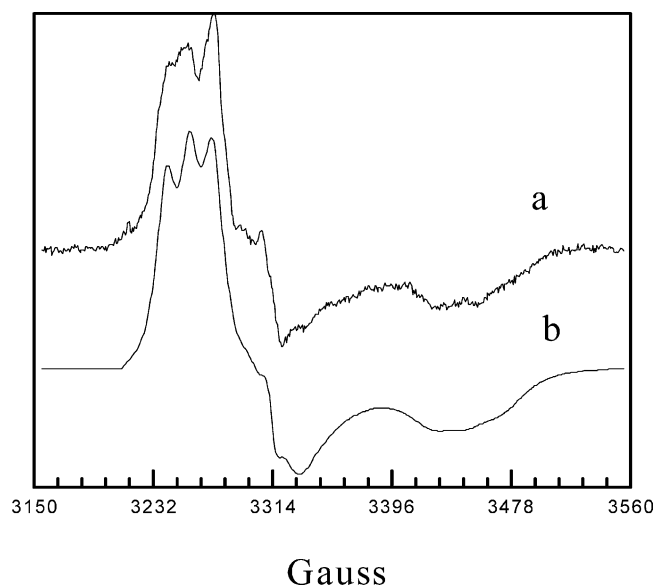


Fig. 9. X-band EPR spectrum at 113 K obtained by reduction of **2d** with CoCp<sub>2</sub> in CH<sub>2</sub>Cl<sub>2</sub>: (a) observed; (b) simulated spectrum.

As for the methylnitrosyl derivatives **3a** and **3b** the experiments do not detect any EPR active species, as was already observed for the electrochemically generated reduction product.

Reduction of the dications **1a**, **1b** and **2d** on a preparative scale has been studied in different solvents. As already stated, because of the poor solubility of the dications in benzene and dichloromethane, cobaltocene is always in a large excess, whatever the Co/Ru molar ratio is. In acetone both reactants are soluble and the molar ratios employed correspond to the relative amounts of the species in solution.

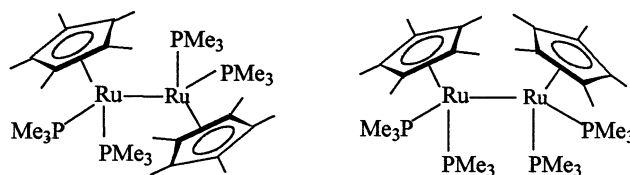
10 minutes after the addition of CoCp<sub>2</sub> in CD<sub>2</sub>Cl<sub>2</sub> (CoCp<sub>2</sub>/Ru molar ratio = 2.5) in the presence of hexamethylbenzene as internal standard, it was found by <sup>1</sup>H-NMR spectroscopy that a mixture of two new products formed in approximately 1/1 ratio, as shown by the presence of two pairs of signals, one consisting of a virtual triplet at  $\delta$  1.42 (vt,  $^2J_{HP} + ^4J_{HP} = 8.8$  Hz, PMe<sub>3</sub>), and a triplet at  $\delta$  1.67 (t,  $J_{HP} = 1.5$  Hz, C<sub>5</sub>Me<sub>5</sub>), the other consisting of a virtual triplet at  $\delta$  1.37 (vt,  $^2J_{HP} + ^4J_{HP} = 8.3$  Hz, PMe<sub>3</sub>) and a triplet at  $\delta$  1.62 (t,  $J_{HP} = 1.5$  Hz, C<sub>5</sub>Me<sub>5</sub>). The amounts of these products increased up to reach a maximum total yield of 71%. In

the meanwhile [CoCp<sub>2</sub>]<sup>+</sup> formed almost double (1.95) that of the initial ruthenium dication, thus showing that an overall two-electrons reduction process has taken place. Although we have not been able to isolate these complexes, on the base of the NMR spectra we propose tentatively the following isomeric (*cis* and *trans*) structures **A** and **B** (Scheme 1).

Some dinuclear non bridged cyclopentadienyl complexes of ruthenium(I) containing a metal–metal bond are reported in the literature such as [Ru<sub>2</sub>Cp<sub>2</sub>(CO)<sub>4</sub>] [17], or the fulvalene complex [( $\eta^5$ : $\eta^5$ -C<sub>10</sub>H<sub>8</sub>)Ru<sub>2</sub>(CO)<sub>4</sub>] and its ring substituted derivatives [18], but in all cases the carbonyl ligand shifts from the terminal to the bridging mode of bonding depending on the experimental conditions.

The reaction was also monitored by IR spectroscopy of the solution in the region of the nitrosyl stretching frequencies. Since [RuCp\*(NO)(PMe<sub>3</sub>)<sub>2</sub>](BF<sub>4</sub>)<sub>2</sub> (**1a**) is insoluble in CH<sub>2</sub>Cl<sub>2</sub>, all the NO bands have to be attributed to soluble reduction products. In the course of 10 minutes a band at 1613 cm<sup>-1</sup> grew, which, by considering also the <sup>1</sup>H-NMR and EPR data, has been attributed to the formation of the one-electron reduction product, [RuCp\*(NO)(PMe<sub>3</sub>)<sub>2</sub>]<sup>•+</sup>. The  $\nu_{NO}$  value (1613 cm<sup>-1</sup>) is much lower than in the case of the starting complex (1845 cm<sup>-1</sup>) [19], and is then indicative of a bent Ru–N–O arrangement (although one must be cautious about such relationship, as will be discussed later) [20].

When the reaction was carried out in (CD<sub>3</sub>)<sub>2</sub>CO, the reduction was quite rapid, being over after 10 min as shown by the amounts of [CoCp<sub>2</sub>]<sup>+</sup> formed ( $\delta$  5.9) and from the absence of the starting compound. The spectrum shows the presence of a mixture of **A** and **B**



**A + B**

Scheme 1.

whose total yield depends on the  $\text{CoCp}_2/\text{Ru}$  molar ratio (23% at  $\text{CoCp}_2/\text{Ru} = 1$ ; 77% at  $\text{CoCp}_2/\text{Ru} = 2$ ).

In contrast the reaction in  $\text{C}_6\text{D}_6$  takes a different path: after a few minutes  $^1\text{H-NMR}$  spectroscopy showed, in addition to a doublet at  $\delta$  0.86 ( $J_{\text{HP}} = 12.8$  Hz) attributable to the trimethylphosphine oxide [8], the formation of two doublets at  $\delta$  1.15 ( $J_{\text{HP}} = 8.75$  Hz) and  $\delta$  1.92 ( $J_{\text{HP}} = 1.2$  Hz) for the  $\text{PMe}_3$  and  $\text{C}_5\text{Me}_5$  ligands, respectively. The multiplicity of the  $\text{C}_5\text{Me}_5$  resonance and the integrated areas of the two signals indicate the presence of one  $\text{PMe}_3$  ligand. Although we could not isolate this compound without extensive decomposition, we identified it as  $[\text{RuCp}^*(\text{NO})(\text{PMe}_3)]$  (**4a**) by comparison with the  $^1\text{H-NMR}$  data reported in the literature for **4a** prepared by thermal decomposition of  $[\text{Ru}(\text{Ph})_2\text{Cp}^*(\text{NO})]$  in the presence of  $\text{PMe}_3$  [21] (Scheme 2).

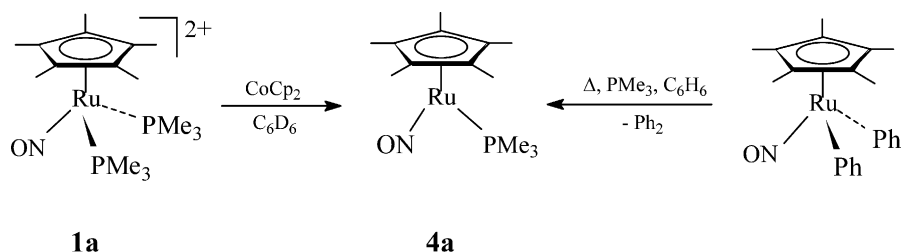
The formation of **4a** can be explained by assuming that, as a consequence of the overall two-electron reduction of **1a**, which is largely localised on the nitrosyl ligand, the co-ordination mode of the  $\text{Ru-N-O}$  system shifts from linear to bent maintaining the 18e configuration. This corresponds formally to the change from the ruthenium(II)/ $\text{NO}^+$  to a ruthenium(II)/NO and then to a ruthenium(II)/ $\text{NO}^-$  system, or, according to the Enemark and Feltham nomenclature [6], from a  $\{\text{RuNO}\}^6-$  to a  $\{\text{RuNO}\}^7-$  and to a  $\{\text{RuNO}\}^8-$ -type nitrosyl derivative. Then the  $\text{Ru-N-O}$  system returns to a linear geometry via the loss of  $\text{PMe}_3$ , giving eventually **4a**, or alternatively the one-electron reduction intermediate releases  $\text{NO}^+$  to yield a 17e fragment which rapidly dimerises to a mixture of the **A** and **B** isomers (Scheme 3) and which can be related to the minor EPR signal observed in Fig. 2. Accordingly to the scheme, the loss of  $\text{NO}^+$  (then formation of dimers) should be, as it is, the favoured reaction pattern in polar solvents such as dichloromethane or acetone, while the overall two-electrons reduction is favoured in benzene, where  $\text{CoCp}_2$  is much more soluble than **1a**.

A similar behaviour was shown by  $[\text{RuCp}^*(\text{NO})(\text{PMe}_2\text{Ph})_2](\text{BF}_4)_2$  (**1b**). By reacting for 12 h a suspension of **1b** in  $\text{C}_6\text{D}_6$  with  $\text{CoCp}_2$  using a molar ratio  $\text{Co}/\text{Ru}$  of 2, we observed a  $^1\text{H-NMR}$  spectrum which was characterised by the presence of a doublet at  $\delta$  1.79 ( $J_{\text{HP}} = 1.1$  Hz) for a  $\text{C}_5\text{Me}_5$  ligand and a doublet at

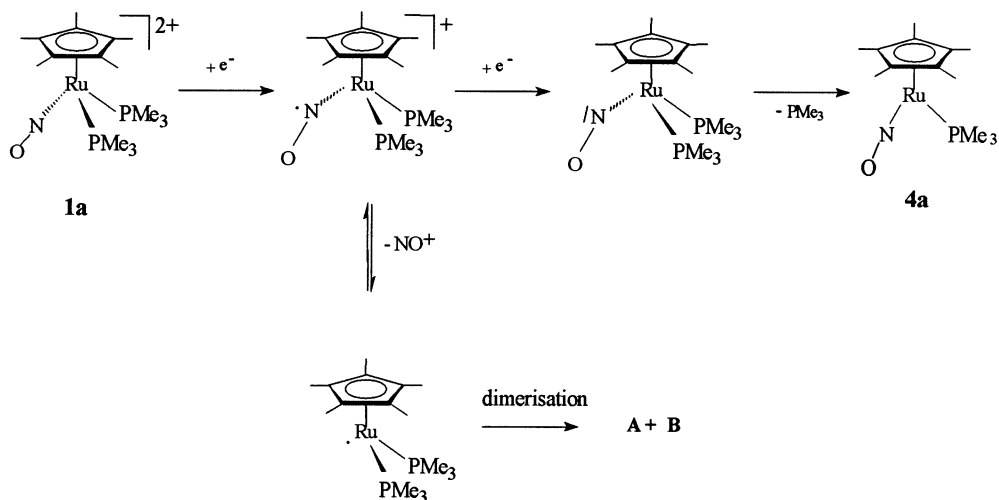
1.45 ( $J_{\text{HP}} = 9.4$  Hz) for the methyl groups of one phosphine ligand. The presence of  $\text{OPMe}_2\text{Ph}$  (doublet at  $\delta$  1.11;  $J_{\text{HP}} = 13.5$  Hz) was also detected. In  $\text{CD}_3\text{COCD}_3$  the reaction is homogeneous and proceeds much more rapidly: after 10 minutes the signals of the initial dication disappeared, and a singlet for  $[\text{CoCp}_2]^+$  was observed at  $\delta$  5.9 together with two doublets at  $\delta$  1.84 and  $\delta$  1.69, due to the  $\text{C}_5\text{Me}_5$  and the  $\text{PMe}_2\text{Ph}$  ligands respectively, having the same coupling constants as in  $\text{C}_6\text{D}_6$ . We propose the structure  $[\text{RuCp}^*(\text{NO})(\text{PMe}_2\text{Ph})]$  (**4b**) by analogy to what observed for the  $\text{PMe}_3$  derivative **4a** (Scheme 4). After two days the  $^1\text{H-NMR}$  signals due to **4b** disappeared. Formation of  $\text{OPMe}_2\text{Ph}$  ( $\delta$  1.10) was observed. The absence of products of the type **A** and **B** in the case of the reaction in acetone may be attributed to the greater cone angle of dimethylphenylphosphine which could be critical for the formation of these species. Monitoring the reaction by IR spectroscopy in  $\text{CH}_2\text{Cl}_2$  shows after 10 minutes a nitrosyl band at  $1636\text{ cm}^{-1}$  which was assigned to the NO band of the one-electron reduction product,  $[\text{RuCp}^*(\text{NO})(\text{PMe}_2\text{Ph})]^+$ .

Addition of cobaltocene to  $[\text{RuCp}(\text{NO})(\text{PPh}_3)_2](\text{BF}_4)_2$  (**2d**) ( $\text{Co}/\text{Ru} = 2$ ) in  $\text{CD}_2\text{Cl}_2$  produced a solution which presents, after 10 minutes, a  $^1\text{H-NMR}$  spectrum where the Cp singlet of **2d** at  $\delta$  6.08 had disappeared, while a new Cp singlet at  $\delta$  4.65 was growing. The area of aromatic protons resulted to be changed showing signals due to free triphenylphosphine ( $\delta$  7.4–7.7). The yield of the new compound was 45%, the amount of  $[\text{CoCp}_2]^+$  being 1.92 times that of the starting complex. The IR spectrum of **2d** in  $\text{CH}_2\text{Cl}_2$  has the NO band at  $1863\text{ cm}^{-1}$ , which disappears after 10 min from the addition of  $\text{CoCp}_2$ , while two new bands at 1670 and  $1691\text{ cm}^{-1}$  arise. These absorptions have been attributed to the one-electron reduction product,  $[\text{RuCp}(\text{NO})(\text{PPh}_3)_2]\text{BF}_4$  and to  $[\text{RuCp}(\text{NO})(\text{PPh}_3)]$  (**5d**) respectively, since the first one decreases during the reaction in favour of the latter. In confirmation of this hypothesis, reaction of **5d** with  $\text{AgBF}_4$  in the presence of an excess of  $\text{PPh}_3$  gives back **2d** (Scheme 5) (as shown by  $^1\text{H-NMR}$  spectroscopy).

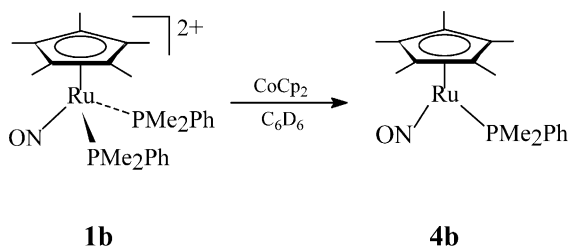
$[\text{RuCp}(\text{NO})(\text{PPh}_3)]$  is not described in literature, but it has been reported that the corresponding pentamethylcyclopentadienyl derivative  $[\text{RuCp}^*(\text{NO})(\text{PPh}_3)]$  has an absorption in the nitrosyl stretching area at 1670



Scheme 2.



Scheme 3.



Scheme 4.

$\text{cm}^{-1}$ , which compares nicely with the value of  $1691 \text{ cm}^{-1}$  for **5d**, taking into account the different Cp ligand [21].

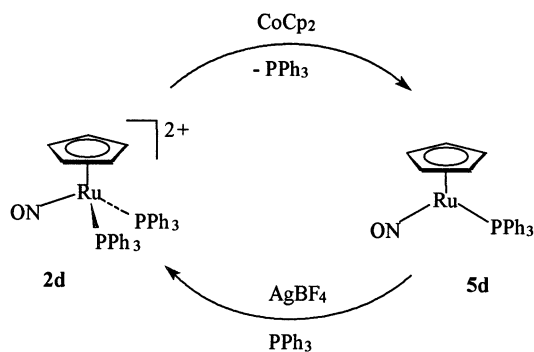
### 2.3. On the geometry of the Ru–N–O moiety

It is well documented how the M–N–O angle varies according to the population of nitrogen orbitals. As known [19], the N–O stretching frequencies in nitrosyl complexes may be diagnostic of the co-ordination mode of the NO ligand, and of the geometry of the M–N–O system, low values suggesting a bent structure and high values a linear one. Unfortunately, in many cases this

method proved to be unreliable because of the large overlap of values which can be diagnostic for both structures ( $1600\text{--}1720 \text{ cm}^{-1}$ ). Haymore and Ibers have proposed empirical rules to correct the observed  $\nu_{\text{NO}}$  stretching wavenumbers in order to choose for linear or bent nitrosyl depending on the  $\nu_{\text{NO}}$  being greater or less than  $1610 \text{ cm}^{-1}$  [20]. On this basis we have corrected the  $\nu_{\text{NO}}$  values for the above nitrosyl complexes together with those of the iridium nitrosyls we have recently reported [7] (Table 3): these data point to a bent geometry in the case of the reduced ruthenium complexes (then NO complexes of ruthenium(II)) and a linear geometry for the iridium case (then  $\text{NO}^+$  complexes of iridium(II)). These conclusions are in nice agreement with the EPR studies which indicate a substantially different behaviour of the iridium and ruthenium systems.

In order to determine the details of the electronic structure and in particular to find theoretical confirmation about the Ru–N–O arrangement inferred from IR data, we carried out DFT calculation of the spin density distribution in these compounds. In order to check the reliability of the method, we have first carried out the theoretical structure determination for the iridium complex  $[\text{Ir}(\text{Me})_2\text{Cp}^*(\text{NO})]\text{BF}_4$  (**6**), which is related to our complexes and whose X-ray crystal structure has been determined (vide infra). The resulting calculated bond lengths and angles agree satisfactorily with the X-ray data (Table 4). In particular the Ir–N–O angle of  $171.84^\circ$  compares well with the observed value of  $171(1)^\circ$ , taking also in account that the calculation results refer to an isolated molecule.

As for  $[\text{RuCp}^*(\text{NO})(\text{PMe}_3)_2]^+$  and  $[\text{RuCp}^*(\text{NO})(\text{PMe}_2\text{Ph})_2]^+$  (the negative spin densities only are represented for the sake of clarity in the spin density maps reported in Fig. 10), the Ru–N–O angles were found to be  $136.2^\circ$  (**1a**,  $172.2^\circ$ ) and  $137.2^\circ$  (**1b**,  $173.3^\circ$ ),



Scheme 5.

Table 3

Experimental ( $\nu$ ) and corrected ( $\nu'$ ) frequencies of the N–O stretching in half-sandwich ruthenium and iridium nitrosyl derivatives

Compound	$\nu$ (cm <sup>-1</sup> )	$\nu'$ (cm <sup>-1</sup> )	Reference
[RuCp*(NO)(PMe <sub>3</sub> ) <sub>2</sub> ] <sup>2+</sup> ( <b>1a</b> )	1845	1675	[8]
[RuCp*(NO)(PMe <sub>3</sub> ) <sub>2</sub> ] <sup>+</sup>	1613	1503	This work
[RuCp*(NO)(PMe <sub>3</sub> )] (4a)	1647	1617	This work
[RuCp*(NO)(PMe <sub>2</sub> Ph) <sub>2</sub> ] <sup>2+</sup> ( <b>1b</b> )	1834	1664	[8]
[RuCp*(NO)(PMe <sub>2</sub> Ph) <sub>2</sub> ] <sup>+</sup>	1636	1526	This work
[RuCp(NO)(PPh <sub>3</sub> ) <sub>2</sub> ] <sup>2+</sup> ( <b>2d</b> )	1863	1693	[8]
[RuCp(NO)(PPh <sub>3</sub> ) <sub>2</sub> ] <sup>+</sup>	1671	1561	This work
[RuCp(NO)(PPh <sub>3</sub> )] (5d)	1691	1661	This work
[Ru(Me)Cp*(NO)(PMe <sub>3</sub> ) <sub>2</sub> ] <sup>+</sup>	1790	1680	[8]
[Ru(Me)Cp*(NO)(PMe <sub>2</sub> Ph)] <sup>+</sup>	1808	1698	[8]
[Ir(Me) <sub>2</sub> Cp*(NO)] <sup>+</sup>	1843	1763	[7]
[Ir(Me)Cp*(NO)(PMe <sub>3</sub> ) <sub>2</sub> ] <sup>2+</sup>	1903	1763	[7]
[Ir(Me)Cp*(NO)(PMe <sub>3</sub> ) <sub>2</sub> ] <sup>+</sup>	1823	1743	[7]
[Ir(Me)Cp*(NO)(PMe <sub>2</sub> Ph)] <sup>2+</sup>	1902	1762	[7]
[Ir(Me)Cp*(NO)(PMe <sub>2</sub> Ph)] <sup>+</sup>	1825	1745	[7]
[Ir(Me)Cp*(NO)(PMePh <sub>2</sub> ) <sub>2</sub> ] <sup>2+</sup>	1900	1760	[7]

respectively, thus confirming nicely the results based on IR spectroscopy.

#### 2.4. Molecular structure of [Ir(Me)<sub>2</sub>Cp\*(NO)]BF<sub>4</sub> (**6**)

We have not been able to obtain crystals of the above ruthenium nitrosyls suitable for X-ray structural studies. We now make reference to literature data and to the related [Ir(Me)<sub>2</sub>Cp\*(NO)]BF<sub>4</sub> (**6**), which forms together with [Ir(Me)Cp\*(PPh<sub>3</sub>)<sub>2</sub>]BF<sub>4</sub>, in roughly equivalent amounts [7c], by reaction of [Ir(Me)<sub>2</sub>Cp\*(PPh<sub>3</sub>)] with NOBF<sub>4</sub> in CH<sub>2</sub>Cl<sub>2</sub>. The two compounds, because of similar solubility properties, crystallize as a 40/60 mixture, with **6** the minor component. However, since the colours of the two compounds are quite different ([Ir(Me)Cp\*(PPh<sub>3</sub>)<sub>2</sub>]BF<sub>4</sub> is yellow while [Ir(Me)<sub>2</sub>Cp\*(NO)]BF<sub>4</sub> is red), it was possible to separate mechani-

Table 4

Selected bond distances (Å) and bond angles (°) in [Ir(Me)<sub>2</sub>Cp\*(NO)]BF<sub>4</sub> (**6**)

	X-ray study <sup>a</sup>	DFT calculation <sup>b</sup>
<i>Bond lengths</i>		
Ir–Cp*	1.919(5)	1.988
Ir–N	1.77 (1)	1.794
Ir–C(7)	2.14 (1)	2.147
N–O	1.13 (2)	1.172
<i>Bond angles</i>		
C(7)–Ir–N	89.9 (5)	90.19
C(7)–Ir–C(7)'	85 (1)	82.15
C(7)–Ir–Cp*	118.1(5)	117.75
Cp*–Ir–N	140.5(5)	141.66
Ir–N–O	171 (1)	171.84

<sup>a</sup> Symmetry transformations used to generate equivalent atoms: ', 1–x, –y+1/2, z.

<sup>b</sup> DFT optimized molecular geometry data.

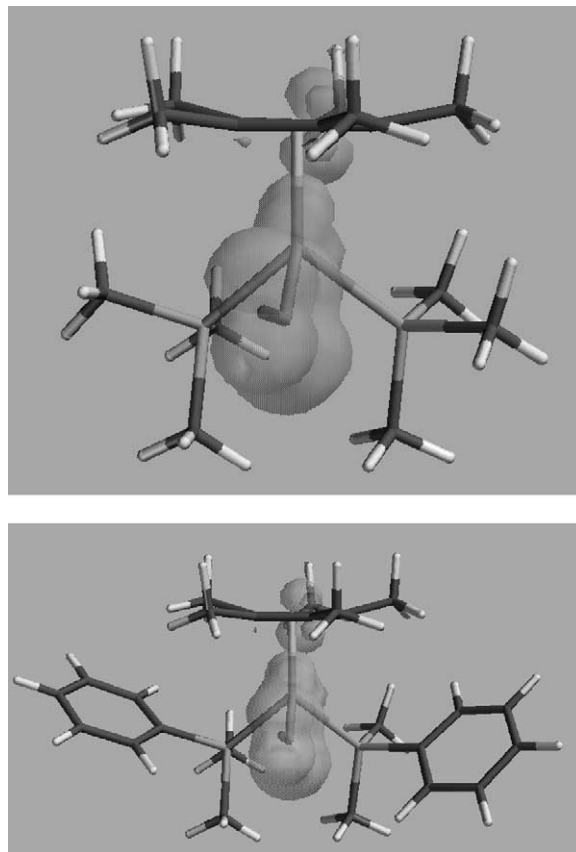


Fig. 10. DFT calculated spin density surfaces (0.002 electron/au<sup>3</sup>) of the radical cations [RuCp\*(NO)(PMe<sub>3</sub>)<sub>2</sub>]<sup>+</sup> (upper) and [RuCp\*(NO)(PMe<sub>2</sub>Ph)<sub>2</sub>]<sup>+</sup> (lower).

cally the two types of crystals. In this way some well shaped red crystals of **6** were collected from a mixture of yellow and red crystals obtained from acetone at –20 °C and the molecular structure was determined by X-ray diffraction measures.

As shown in Fig. 11, the cation presents a pseudo-octahedral hexacoordinated symmetry (bond angles around the iridium atom are close to 90°), where the pentamethylcyclopentadienyl ligand occupies three coordination sites around the metal, and the nitrosyl and two methyls occupy the remaining three sites: this is a situation rather typical for compounds of general formula [IrCp\*(L)<sub>3</sub>] [22].

As far as we know, crystal structures of iridium(III) nitrosyl complexes have not yet been reported in the literature apart from the bent nitrosyl complex [IrCl(PPh<sub>3</sub>)<sub>2</sub>(CO)(NO)]<sup>+</sup> [23], which is a nitrosyl derivative with a bent Ir–N–O moiety, then formally an iridium(III) complex. Comparison can be made with the related ‘half sandwich’ iridium(I) derivative [IrCp\*(NO)(C<sub>2</sub>H<sub>4</sub>)]BF<sub>4</sub>, (Ir–N 1.762(9) Å; N–O 1.15(1) Å; Ir–N–O 175.8(9)° ( $\nu_{\text{NO}}$  = 1822 cm<sup>-1</sup>) [24].

Selected bond distances (Å) and angles (°) are reported in Table 4.

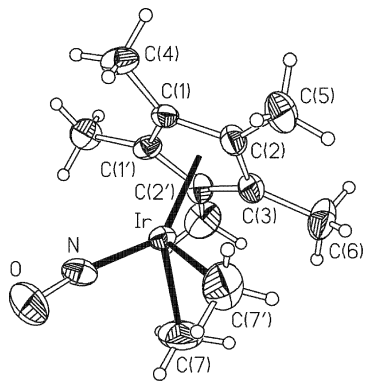


Fig. 11. X-ray crystal structure of  $[\text{Ir}(\text{Me})_2\text{Cp}^*(\text{NO})]^+$  with atom labeling.

As can be noticed from the tabulated data, the bond angle ( $\text{Ir}-\text{N}-\text{O}$   $170.71^\circ$ ) and IR stretching frequency ( $\nu_{\text{NO}} = 1843 \text{ cm}^{-1}$ ) are in agreement with an essentially linear structure for the  $\text{Ir}-\text{N}-\text{O}$  system.

### 3. Conclusion

Electrochemical studies show that the dicationic **1a**, **1b** and **2d** undergo facile two one-electron reduction steps, although only in the case of **1a** the stability of the reduced species is sufficient to give clean patterns. EPR characterization of the reduced species indicate that the extra electron is predominantly centred on the nitrosyl ligand. Analogous results have been obtained by chemical reduction, then identifying the one-electron reduction products as 18e complexes. In particular IR spectroscopy together with DFT calculations indicate that the  $\text{Ru}-\text{N}-\text{O}$  moiety is bent. The reduced complexes are not stable and they rearrange by releasing a phosphine or a NO ligand in a way depending on the nature of the ancillary ligands and on the experimental conditions.

### 4. Experimental

The reactions and manipulation of organometallics were carried out under dinitrogen or argon, using standard techniques. The solvents were dried and distilled prior to use.  $[\text{RuCp}^*(\text{NO})(\text{L})_2](\text{BF}_4)_2$  ( $\text{L} = \text{PMe}_3$ , **1a**;  $\text{PMe}_2\text{Ph}$ , **1b**),  $[\text{RuCp}(\text{NO})(\text{PPh}_3)_2](\text{BF}_4)_2$  (**2d**) and  $[\text{Ru}(\text{Me})\text{Cp}^*(\text{NO})(\text{L})]\text{BF}_4$  ( $\text{L} = \text{PMe}_3$ , **3a**;  $\text{PMe}_2\text{Ph}$ , **3b**) were prepared according to published procedures [8].  $\text{NOBF}_4$  (Aldrich product) was treated under vacuum before use.  $\text{CoCp}_2$  (Aldrich) was freshly sublimed prior to use.  $[\text{Ir}(\text{Me})_2\text{Cp}^*(\text{NO})]\text{BF}_4$  was prepared as described [7c]. Infrared spectra were recorded on a FT-IR Perkin Elmer 1750 instrument.  $^1\text{H-NMR}$  spectra were recorded on Varian Gemini 200 and VXR

300 instruments. Material and apparatus used for electrochemistry and coupled EPR measurements have been described elsewhere [25]. All the potentials values are referred to the saturated calomel electrode (SCE): under the present experimental conditions the one-electron oxidation of ferrocene occurs at  $+0.38 \text{ V}$  (acetone). EPR spectra for the study of chemical reductions were obtained by using EPR Varian E 112 instrument equipped with a Varian E 257 for temperature control. The spectrometer was interfaced to an AST Premium 486/25 by means of a data acquisition system capable of acquiring up to 500 000 12-bit samples  $\text{s}^{-1}$ , including 32-bit add to memory, thus giving on-line signal averaging and a software package specially designed for EPR experiments [26]. Full optimization of the molecular geometries of the cation and cation radical species and calculation of the electron spin density distributions and surfaces were carried out using the UNIX version of SPARTAN 5.1.3 computer program [27] running on a Digital/Compaq workstation. DFT data were obtained by adopting the p-BP86 scheme that uses the functional proposed by Becke [28] and the Perdew [29] correlation functional, adopting the DN\*\* base functions set, which is appropriate for calculations of split-valence-plus-polarization quality.

#### 4.1. Reaction of $[\text{RuCp}^*(\text{NO})(\text{PMe}_3)_2](\text{BF}_4)_2$ (**1a**) with $\text{CoCp}_2$

##### 4.1.1. General procedure

Reduction of **1a** was carried out in a NMR tube. The tube was inserted into an Ace NMR-tube tip-off manifold, connected to a vacuum line and degassed; then it was cooled and charged with the reactants and the solvent, and finally was tipped off with flame. The reaction was done in dichloromethane, acetone and in benzene, using equimolar amounts of reagents or an excess of  $\text{CoCp}_2$ .

##### 4.1.2. In $\text{CD}_2\text{Cl}_2$ , $\text{Co/Ru} = 2.5$

Complex **1a** (0.010 g, 0.017 mmol) was reacted with  $\text{CoCp}_2$  (0.008 g, 0.043 mmol) in  $\text{CD}_2\text{Cl}_2$  (1 ml) in the presence of  $\text{C}_6\text{Me}_6$  (0.002 g, 0.0122 mmol) as internal standard. After 30 min the deep-maroon solution was examined by  $^1\text{H-NMR}$  spectroscopy, which showed the formation (in addition to the  $\text{CoCp}_2^+$  resonance at  $\delta$  5.72) of two groups of signals assigned to the new compounds A and B (71% yield).  $^1\text{H-NMR}$  ( $\text{CD}_2\text{Cl}_2$ ):  $\delta$  1.42 (18H, vt,  $J_{\text{HP}} = 8.2 \text{ Hz}$ ,  $\text{PMe}_3$ ), 1.67 (15H, t,  $^2J_{\text{HP}} + ^4J_{\text{HP}} = 1.5 \text{ Hz}$ ,  $\text{C}_5\text{Me}_5$ ).  $\delta$  1.37 (18H, vt,  $J_{\text{HP}} = 8.5 \text{ Hz}$ ,  $\text{PMe}_3$ ), 1.62 (15H, t,  $^2J_{\text{HP}} + ^4J_{\text{HP}} = 1.5 \text{ Hz}$ ,  $\text{C}_5\text{Me}_5$ ).

##### 4.1.3. In $(\text{CD}_3)_2\text{CO}$ , $\text{Co/Ru} = 2$

Since the reaction proceeded without substantial variations using a molar ratio  $\text{Co/Ru} = 1$  or 2, we report

as an example only the results under a reducing agent/ruthenium molar ratio = 2. CoCp<sub>2</sub> (0.008 g, 0.042 mmol) was added to a solution of **1a** (0.013 g, 0.021 mmol) in CD<sub>3</sub>COCD<sub>3</sub> (1 ml) and C<sub>6</sub>Me<sub>6</sub> (0.002 g, 0.014 mmol), as internal standard. After 30 min the <sup>1</sup>H-NMR spectrum showed the formation of **A** and **B** (77%). <sup>1</sup>H-NMR ((CD<sub>3</sub>)<sub>2</sub>CO): δ 1.43 (18H, vt, PMe<sub>3</sub>), 1.68 (15H, t, C<sub>5</sub>Me<sub>5</sub>). δ 1.38 (18H, vt, PMe<sub>3</sub>), 1.62 (15H, t, *J*<sub>HP</sub> = 1.5 Hz, C<sub>5</sub>Me<sub>5</sub>).

#### 4.1.4. In C<sub>6</sub>D<sub>6</sub>, Co/Ru = 2

Complex **1a** (0.023 g, 0.039 mmol) in C<sub>6</sub>D<sub>6</sub> (1 ml) was reacted with CoCp<sub>2</sub> (0.015 g, 0.080 mmol). The mixing of the reactants was followed by the formation of a maroon suspension. After 20 min [RuCp\*(NO)(PMe<sub>3</sub>)] (**4a**) was formed as identified by the comparison of the <sup>1</sup>H-NMR spectrum with that of an authentic sample prepared via a different route [8]. <sup>1</sup>H-NMR (C<sub>6</sub>D<sub>6</sub>): δ 1.15 (9H, d, *J*<sub>HP</sub> = 8.9 Hz, PMe<sub>3</sub>), 1.92 (15H, d, *J*<sub>HP</sub> = 1.2 Hz, C<sub>5</sub>Me<sub>5</sub>). Equivalent amounts of trimethylphosphine oxide (δ 0.86, d, *J* = 12.8 Hz) were formed. The organometallic product reached a maximum after a few hours, then slowly decreased during a 24-h period. The signals due to **A** and **B** appeared being largely predominant after 24 h. These products (in a 3/2 ratio) were still present after 4 days at room temperature (r.t.). <sup>1</sup>H-NMR (C<sub>6</sub>D<sub>6</sub>): δ 1.22 (18H, d, PMe<sub>3</sub>), 1.56 (15H, t, C<sub>5</sub>Me<sub>5</sub>). δ 1.18 (18H, d, PMe<sub>3</sub>), 1.53 (15H, t, C<sub>5</sub>Me<sub>5</sub>).

#### 4.2. Reaction of [RuCp\*(NO)(PMe<sub>2</sub>Ph)<sub>2</sub>](BF<sub>4</sub>)<sub>2</sub> (**1b**) with CoCp<sub>2</sub>: formation of [RuCp\*(NO)(PMe<sub>2</sub>Ph)] (**4b**)

In a <sup>1</sup>H-NMR tube CoCp<sub>2</sub> (0.010 g, 0.053 mmol) was added to a suspension of **1b** (0.016 g, 0.023 mmol) in C<sub>6</sub>D<sub>6</sub> (1 ml). After 40 min the spectrum showed new signals consistent with the structure [RuCp\*(NO)(PMe<sub>2</sub>Ph)] (**4b**) and with dimethylphenylphosphine oxide (δ 1.10, d, *J* = 13.5 Hz). <sup>1</sup>H-NMR: δ 1.45 (6H, d, *J*<sub>HP</sub> = 9.4 Hz, PMe<sub>2</sub>Ph), 1.79 (15H, d, *J*<sub>HP</sub> = 1.1 Hz, C<sub>5</sub>Me<sub>5</sub>), 7.45–7.70 (15H, m, PPh). The same procedure was followed in (CD<sub>3</sub>)<sub>2</sub>CO. <sup>1</sup>H-NMR: δ 1.69 (6H, d, PMe<sub>2</sub>Ph), 1.84 (15H, d, C<sub>5</sub>Me<sub>5</sub>).

#### 4.3. Reaction of [RuCp(NO)(PPh<sub>3</sub>)<sub>2</sub>](BF<sub>4</sub>)<sub>2</sub> (**2d**) with CoCp<sub>2</sub>: formation of [RuCp(NO)(PPh<sub>3</sub>)] (**5d**)

Complex **2d** (0.018 g, 0.02 mmol) in CD<sub>2</sub>Cl<sub>2</sub> (1 ml) was treated in a <sup>1</sup>H-NMR tube with CoCp<sub>2</sub> (0.008 g, 0.043 mmol). After 10 min the <sup>1</sup>H-NMR spectrum showed the formation of a new product displaying resonances at δ 4.65 (5H, s, C<sub>5</sub>H<sub>5</sub>) and 7.4–7.85 (30H, m, PPh<sub>3</sub>), tentatively identified as [RuCp(NO)(PPh<sub>3</sub>)] (**5d**) in a 50% yield (evaluated on the basis of the CoCp<sub>2</sub><sup>+</sup> resonance at δ 6.1). The product underwent decomposi-

tion at room temperature leading to new cyclopentadienyl derivatives and free phosphine (δ 7.2–7.4).

#### 4.4. EPR spectral studies of the reactions of the nitrosyl derivatives with CoCp<sub>2</sub>

A weighed amount of metal complex (typically 5 mg) and CoCp<sub>2</sub> (Co/Ru = 2) was placed into a quartz tube (o.d. 3 mm; i.d. 2 mm) fitted with a quartz-Pyrex joint and a Corning Rotaflo Teflon tap (DISA, Milan). The tube was attached to a vacuum line and degassed by standard vacuum/argon techniques; then it was immersed in a dry ice-cooled acetone bath and charged with dichloromethane. The quartz tube was then introduced into the spectrometer cavity, pre-cooled to the desired temperature, and the reagents were allowed to mix gradually. The hyperfine coupling constants and linewidths were obtained by computer simulation of the EPR spectra.

#### 4.5. X-ray crystallographic studies

The X-ray diffraction measurements were carried out at room temperature by means of a Bruker P4 diffractometer equipped with a graphite-monochromated Mo–K<sub>α</sub> radiation. A splinter of dimensions 0.44 × 0.44 × 0.26 mm<sup>-3</sup>, cut from a red–brown prismatic crystal was sealed in a glass capillary under an argon atmosphere. The unit cell parameters are listed in Table 1. The intensity data collection was carried out with the ω–2θ scan mode, collecting a redundant set of data; index ranges: –8 ≤ *h* ≤ 1, –17 ≤ *k* ≤ 1, –9 ≤ *l* ≤ 9. Three standard reflections were measured every 97 measurements to check the sample decay. The intensities were corrected for Lorentz and polarisation effects and for absorption by means of a ψ-scan method [30]. The systematic absences suggested the presence of only a screw axis and, taking into account the intensity data statistics, the structure solution was conducted in the centrosymmetric *P*2<sub>1</sub>/*m* space group by means of the automatic direct methods contained in the SHELX-97 programme [31]. Both ions were placed in special positions: the cation in the Wyckoff position *e* (site symmetry *m*) and the anion in the position *b* (site symmetry  $\bar{1}$ ). While the cation [Ir(Me)<sub>2</sub>Cp\*(NO)]BF<sub>4</sub> can display a mirror, the tetrahedral anion is not compatible with the  $\bar{1}$  operator, so that a statistical distribution of the anion on two centrosymmetrically related positions is obtained. In order to check whether the anion disorder is real, the structure refinement was tried both in the *P*2<sub>1</sub>/*m* and in *P*2<sub>1</sub> space groups. The non centrosymmetric space group was then excluded because, notwithstanding the almost double number of variables, its assumption neither removed the anion disorder nor improved the reliability factor *R*. The final refinement cycle with full-matrix least-squares based on

Table 5  
Crystal data and structure refinement for [Ir(Me)<sub>2</sub>Cp\*(NO)]BF<sub>4</sub>

Empirical formula	C <sub>12</sub> H <sub>21</sub> BF <sub>4</sub> IrNO
Formula weight	474.31
Temperature (K)	293(2)
Wavelength (Å)	0.71073
Crystal system	Monoclinic
Space group	<i>P</i> 2 <sub>1</sub> / <i>m</i>
Unit cell dimensions	
<i>a</i> (Å)	7.347(2)
<i>b</i> (Å)	14.780(3)
<i>c</i> (Å)	8.001(2)
β (°)	114.19(3)
<i>V</i> (Å <sup>3</sup> )	792.5(3)
<i>Z</i>	2
<i>D</i> <sub>calc</sub> (Mg m <sup>-3</sup> )	1.988
Absorption coefficient (mm <sup>-1</sup> )	8.458
<i>F</i> (000)	452
θ Range for data collection (°)	2.76–25.00
Reflections collected	1954
Independent reflections	1451 [ <i>R</i> <sub>int</sub> = 0.0536]
Completeness to θ = 25.00°	99.9%
Data/restraints/parameters	1451/0/109
Goodness-of-fit <sup>a</sup> on <i>F</i> <sup>2</sup>	1.104
Final <i>R</i> indices [ <i>I</i> > 2σ( <i>I</i> )]	<i>R</i> <sub>1</sub> = 0.0409, <i>R</i> <sub>2</sub> = 0.1016
<i>R</i> indices (all data)	<i>R</i> <sub>1</sub> = 0.0488, <i>R</i> <sub>2</sub> = 0.1059
Largest difference peak and hole (e Å <sup>-3</sup> )	1.697 and -1.473

<sup>a</sup> Goodness-of-fit =  $[\sum[w(F_o^2 - F_c^2)^2]/(N - P)]^{1/2}$ , where *N* and *P* are the numbers of observations and parameters, respectively,  $R_1 = \sum||F_o| - |F_c||/\sum|F_o|$ ;  $wR_2 = [\sum[w(F_o^2 - F_c^2)^2]/\sum[w(F_o^2)^2]]^{1/2}$ ;  $w = 1/[\sigma^2(F_o^2) + (AQ)^2 + BQ]$  where  $Q = [\text{MAX}(F_o^2, 0) + 2F_c^2]/3$ .

*F*<sup>2</sup> was performed with anisotropic thermal factors for all heavy atoms, with hydrogen atoms placed in calculated positions. The final reliability factors are listed in Table 5. Data reduction of measured intensities was done by the XSCANS package [32]. Some other utilities contained in the WINGX suite [33] were also used.

## 5. Supplementary material

Crystallographic data for the structural analysis have been deposited with the Cambridge Crystallographic Data Centre, CCDC no. 198177. Copies of this information may be obtained free of charge from The Director, CCDC, 12 Union Road, Cambridge CB2 1EZ, UK (Fax: +44-1223-336033; e-mail: deposit@ccdc.cam.ac.uk or www: <http://www.ccdc.cam.ac.uk>).

## Acknowledgements

We thank CNR (Rome) for financial support.

## References

- [1] (a) K.K. Pandey, *Coord. Chem. Rev.* 51 (1983) 69; (b) V. Zang, R. van Eldik, *Inorg. Chem.* 29 (1990) 4462; (c) G.B. Richter-Addo, P. Legzdins, *Metal Nitrosyls*, Oxford University Press, New York, 1992; (d) E.K. Pham, S.G. Chang, *Nature* 369 (1994) 139.
- [2] (a) J.B. Howard, D.C. Rees, *Chem. Rev.* 96 (1996) 2965; (b) B.K. Burgess, D.J. Lowe, *Chem. Rev.* 96 (1996) 2983; (c) R.R. Eady, *Chem. Rev.* 96 (1996) 3013.
- [3] (a) J.S. Stampler, D.J. Singel, J. Loscalzo, *Science* 258 (1992) 1898; (b) S. Pfeiffer, B. Mayer, B. Hemmens, *Angew. Chem. Int. Ed. Engl.* 38 (1999) 1714; (c) D.R. Lang, J.A. Davis, L.G.F. Lopes, A.A. Ferro, L.C.G. Vasconcelos, D.W. Franco, E. Tfouni, A. Wieraszko, M.J. Clarke, *Inorg. Chem.* 39 (2000) 2294.
- [4] G.B. Richter-Addo, P. Legzdins, J. Burstyn, *Chem. Rev.* 102 (2002) 4.
- [5] (a) J.S. Yu, R.A. Jacobson, R.J. Angelici, *Inorg. Chem.* 21 (1982) 3106; (b) W.E. Geiger, P.H. Reiger, B. Tulythan, M.D. Rausch, *J. Am. Chem. Soc.* 106 (1984) 7000; (c) D. Sellmann, H. Kunstmann, M. Moll, F. Knoch, *Inorg. Chim. Acta* 154 (1988) 157; (d) W.E. Geiger, *Acc. Chem. Res.* 28 (1995) 351; (e) F. Baumann, W. Kaim, L.M. Baraldo, L.D. Slep, J.A. Olabe, J. Fiedler, *Inorg. Chim. Acta* 285 (1999) 129; (f) D. Sellmann, N. Blum, F.W. Heinemann, B.A. Hess, *Chem. Eur. J.* 7 (2001) 1874.
- [6] (a) J.H. Enemark, R.D. Feltham, *Coord. Chem. Rev.* 13 (1974) 339; (b) R.D. Feltham, J.H. Enemark, *Top. Stereochem.* 12 (1981) 155.
- [7] (a) P. Diversi, V. Ermini, G. Ingrosso, A. Lucherini, C. Pinzino, F. Simoncini, *J. Organomet. Chem.* 555 (1998) 135; (b) P. Diversi, M. Fuligni, S. Matteoni, C. Pinzino, 5<sup>o</sup> Convegno Nazionale GIRSE, Rimini, Italy, October 1998; (c) P. Diversi, F. Fabrizi de Biani, G. Ingrosso, F. Laschi, A. Lucherini, C. Pinzino, P. Zanello, *J. Organomet. Chem.* 584 (1999) 73.
- [8] P. Diversi, M. Fontani, M. Fuligni, F. Laschi, S. Matteoni, C. Pinzino, P. Zanello, *J. Organomet. Chem.* 626 (2001) 145 (and references therein).
- [9] (a) R.W. Callahan, T.J. Meyer, *Inorg. Chem.* 16 (1977) 574; (b) M.G. Gomes, C. Davanzo, S.C. Silva, L.G.F. Lopes, P.S. Santos, D.W. Franco, *J. Chem. Soc. Dalton Trans.* (1998) 601; (c) Y. Chen, F.-T. Lin, R.E. Shepherd, *Inorg. Chem.* 38 (1999) 973; (d) H. Nagao, N. Nagao, Y. Yukawa, D. Ooyama, Y. Sato, T. Oosawa, H. Kuroda, F.S. Howell, M. Mukaida, *Bull. Chem. Soc. Jpn.* 72 (1999) 1273; (e) B. Mondal, H. Paul, V.G. Puranik, G.K. Lahiri, *J. Chem. Soc. Dalton Trans.* (2001) 481; (f) B.R. McGarvey, A.A. Ferro, E. Tfouni, C.W.B. Bezerra, I. Bagatin, D.W. Franco, *Inorg. Chem.* 39 (2000) 3577.
- [10] K. Aoyagi, M. Mukaida, H. Kakihana, K. Shimizu, *J. Chem. Soc. Dalton Trans.* (1985) 1733.
- [11] R.W. Callahan, G.M. Brown, J.M. Meyer, *J. Am. Chem. Soc.* 97 (1975) 894.
- [12] E.R. Brown, J.R. Sandifer, in: B.W. Rossiter, J.F. Hamilton (Eds.), *Physical Methods of Chemistry: Electrochemical Methods*, vol. 2, Wiley, New York, 1986.
- [13] A. Ceccanti, P. Diversi, G. Ingrosso, F. Laschi, A. Lucherini, S. Magagna, P. Zanello, *J. Organomet. Chem.* 526 (1996) 251.
- [14] J.P. Lozos, B.M. Hoffman, C.G. Franz, *QCPE* 11 (1973) 243.

- [15] F.E. Mabbs, D. Collison, Electron paramagnetic resonance of d transition metal compounds, in: *Studies in Inorganic Chemistry Series*, vol. 16, Elsevier, New York, 1992.
- [16] (a) The software was provided by the Illinois EPR Research Center, NIH Division of research, Resonances grant. no RR01811;  
(b) K.J. Mattson, R.B. Clarkson, R.L. Belford, 11th International EPR Symposium, 30th Rocky Mountains Conference, Denver, CO, August 1988.
- [17] T.E. Bitterwolf, *Coord. Chem. Rev.* 206 (2000) 419.
- [18] (a) K.P.C. Vollhardt, T.W. Weidman, *J. Am. Chem. Soc.* 105 (1983) 1676;  
(b) T.E. Bitterwolf, *J. Organomet. Chem.* 312 (1986) 197;  
(c) P.E. Bloyce, A.K. Campen, R.H. Hooker, A.J. Rest, N.R. Thomas, T.E. Bitterwolf, J.E. Shade, *J. Chem. Soc. Dalton Trans.* (1990) 2833;  
(d) R.J. Haines, in: D.F. Shriver, M.I. Bruce (Eds.), *Comprehensive Organometallic Chemistry*, Ch. 11, vol. 7, 2nd ed., Pergamon Press, New York, 1995.
- [19] (a) N.N. Greenwood, A. Earnshaw, *Chemistry of the Elements*, Pergamon Press, New York, 1989;  
(b) D. Michael, P. Mingos, D.J. Sherman, *Adv. Inorg. Chem.* 34 (1989) 293.
- [20] (a) B.L. Haymore, J.A. Ibers, *Inorg. Chem.* 14 (1975) 3060;  
(b) A.P. Gaughan, B.L. Haymore, J.A. Ibers, W.H. Myers, T.F. Nappier, D.W. Meek, *J. Am. Chem. Soc.* 95 (1992) 6859;  
(c) K.K. Pandey, *Coord. Chem. Rev.* 121 (1992) 1.
- [21] J. Chang, R.G. Bergman, *J. Am. Chem. Soc.* 109 (1987) 4298.
- [22] (a) L. Andreucci, P. Diversi, G. Ingrosso, A. Lucherini, F. Marchetti, V. Adovasio, M. Nardelli, *J. Chem. Soc. Dalton Trans.* (1986) 477;  
(b) L. Andreucci, P. Diversi, G. Ingrosso, A. Lucherini, F. Marchetti, V. Adovasio, M. Nardelli, *J. Chem. Soc. Dalton Trans.* (1986) 803.
- [23] (a) D.J. Hodgson, J.A. Ibers, *Inorg. Chem.* 7 (1968) 2345;  
(b) D.J. Hodgson, J.A. Ibers, *Inorg. Chem.* 8 (1969) 1282.
- [24] R.J. Batchelor, F.W.B. Einstein, N.D. Lowe, B.A. Palm, X. Yan, D. Sutton, *Organometallics* 13 (1994) 2041.
- [25] D. Osella, M. Ravera, C. Nervi, C.E. Housecroft, P.R. Raithby, P. Zanello, F. Laschi, *Organometallics* 10 (1991) 3253.
- [26] R. Ambrosetti, D. Ricci, *Rev. Sci. Instrum.* 62 (1991) 2281.
- [27] SPARTAN version 5.1.3, Wavefunction Inc., Irvine, CA.
- [28] A.D. Beche, *Phys. Rev. A* 38 (1988) 3098.
- [29] J.P. Perdew, *Phys. Rev. B* 33 (1986) 8822.
- [30] C.T. North, C. Phillips, F.S. Mathews, *Acta Crystallogr. Sect. A* 24 (1968) 351.
- [31] G.M. Sheldrick, *SHELXTL-PLUS*, rel. 5.1, Siemens Analytical X-ray Instruments Inc., Madison, WI, 1997.
- [32] *XSCANS*, X-ray Single Crystal Analysis System, rel. 2.1 Siemens Analytical X-ray Instruments Inc., Madison, WI, 1994.
- [33] L.J. Farrugia, *J. Appl. Crystallogr.* 32 (1999) 837.